ADVANCED MATERIALS INTERFACES
www.advmatinterfaces.de

Fibroblast Response to Nanocolumnar TiO_2 Structures Grown by Oblique Angle Sputter Deposition

Uta Kapprell, Sabrina Friebe, Susann Grüner, Christoph Grüner, Astrid Kupferer, Bernd Rauschenbach, and Stefan G. Mayr**

Cells are established to sense and respond to the properties, including nano- and microscale morphology, of the substrate they adhere to, which opens up the possibility to tailor bioactivity. With this background, the potential of tilted TiO_2 nanostructures grown by oblique angle sputtering to affect fibroblasts with particular focus on inducing anisotropy in cell behavior is explored. By depositing TiO_2 at different oblique angles relative to the substrate normal, morphologies, columnar tilt angle, roughness, and distances between neighbored nanocolumns can be adjusted. To assess bioactivity of the resulting structures, L929-mouse fibroblasts are seeded in vitro on TiO_2 nanostructured substrates. Angle-dependent movement and velocity distributions of the cells on differently tilted columns and a smooth reference sample are studied. Cell proliferation rates and cell areas are additional factors which provide information about viability and the well-being of cells. It could be shown that the local topography of the surface has an influence on the directed movement of the cells.

1. Introduction

Nanostructured TiO_2 thin films have been in the focus of considerable research activities, since those films are essential for a large number of applications such as, antireflective coatings, gas sensing, photo-catalysis, and antibacterial coatings.[1–11] In recent years, nanostructured TiO_2 thin films have become of high interest for coatings of implants. Titanium and its alloys are typically used as materials for hard tissue replacements such as, bone screws and anchoring, hip joint replacements, stents, and fracture fixation devices.[12–15] The biocompatibility of Ti originates from the chemically passive oxide layer naturally forming on the Ti surface.[13] Previous research indicates that the surface properties such as, composition, hydrophilicity, and texture of the oxide on the Ti affect the cellular response. The micro- and nanoscale surface morphology has shown to be a highly-sensitive parameter that influences for instance cell adherence, proliferation, migration, gene expression, and differentiation.[16–23] Therefore, modifying the implant surface on the micro- and nanometer scale appears to be a promising approach for improving the interaction between tissue and implant.[20,24–29]

Various deposition methods are known to fabricate such thin TiO_2 films and comprise chemical (anodic oxidation, spray pyrolysis, chemical vapor deposition, etc.) or physical (DC or RF magnetron sputtering, ion-beam assisted sputtering, electron beam evaporation) approaches. Sputtering is widely used in research and industry due to the low vacuum requirements. Combining sputtering with an oblique angle deposition (OAD) geometry allows tailoring self-assembled, 3D nano- and microstructures over large substrate areas.[30] OAD is a physical vapor deposition technique based on the inter-columnar shadowing effect, which emerges from tilting the substrate normal to highly oblique angles with respect to the incoming vapor.[31–33] This deposition geometry results in the formation of a highly porous thin film that consists of nano-sized columns inclined toward the incoming particle flux. Moreover, these columns are separated from each other so that the resulting thin film exhibits an open pore-structure. These nanostructures might be beneficial for cell adhesion. For instance, Dolatshahi-Pirouz et al. and Pennisi et al. have reported that nanostructured platinum surfaces have a profound impact on the proliferation of primary human fibroblasts, suggesting that nanostructured surfaces affect cellular responses.[34,35] Although being in the focus of considerable research activities, the interactions of cells and such nanostructured surfaces still remain incompletely understood.

In the present work, thin films composed of tilted TiO_2 nanostructures are fabricated by oblique angle ion-beam sputter deposition at room temperature. The columnar tilt angles, the distance between neighbored nanostructures, as well as, the roughness of the thin films were investigated with scanning electron microscopy (SEM) and atomic force microscopy

U. Kapprell, S. Friebe, Dr. S. Grüner, Dr. C. Grüner, A. Kupferer, Prof. S. G. Mayr
Leibniz Institute of Surface Engineering (IOM)
Permoserstraße 15, 04318 Leipzig, Germany
E-mail: sabrina.friebe@iom-leipzig.de; stefan.mayr@iom-leipzig.de
S. Friebe, A. Kupferer, Prof. S. G. Mayr
Division of Surface Physics
Linnéstraße 5, 04103 Leipzig, Germany
Prof. B. Rauschenbach
Innovative Surface Technologies (IOT)
Permoserstraße 15, 04318 Leipzig, Germany
The ORCID identification number(s) for the author(s) of this article can be found under https://doi.org/10.1002/admi.202100646.

DOI: 10.1002/admi.202100646

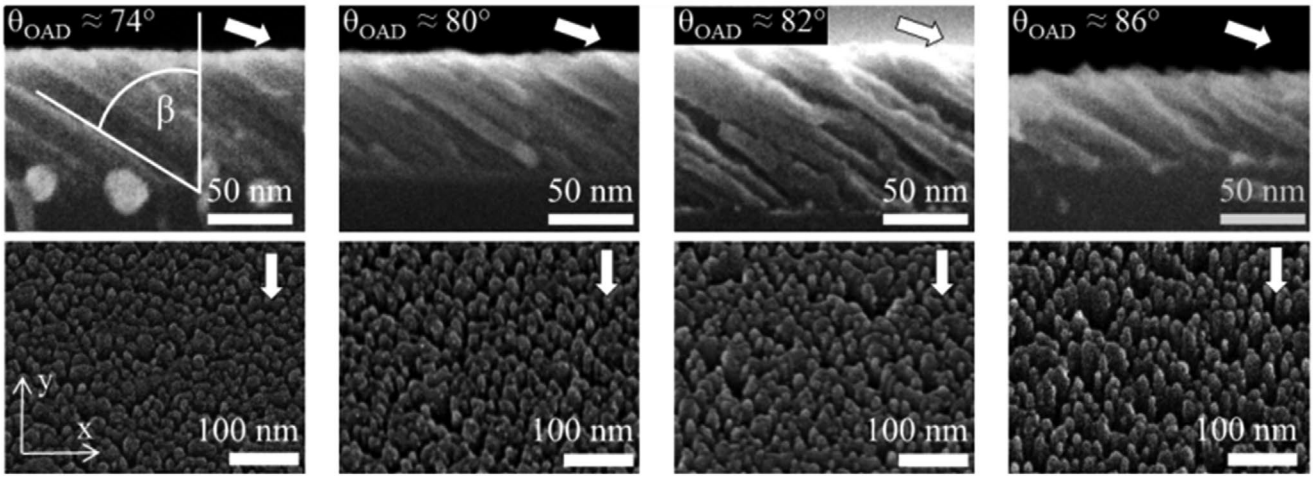

Figure 1. Side view and corresponding top view SEM images of tilted TiO_2 nanostructures deposited for varying incidence angles θ_{OAD} on natively oxidized Si(100) substrates at room temperature. The columnar tilt angle (measured with respect to the substrate normal) is depicted by β. The white arrows indicate the direction of the incoming particle flux.

(AFM). Long-term phase contrast observations of the cellular response on the surface structure effects are in the focus of this study. Especially, the migration of L929 fibroblasts, their resulting angle-dependent movements and velocities as well as cell division rates and cell areas are studied on top of the tilted TiO_2 nanostructured surfaces grown on Si-substrates, exemplarily for in vitro cell culture.

2. Results and Discussion

2.1. Characterization of the Nanostructured TiO_2 Thin Films

Tilted TiO_2 nanostructures are grown on natively oxidized Si(100)-substrates at room temperature and with varying angular positions θ_{OAD} of the sample holder. **Figure 1** gives an overview of such nanostructured thin films. In general, the SEM top-view images reveal that for more oblique deposition geometry, the distance between neighbored nanostructures is increased, thereby reducing the bundling of the columns. This is caused by the shadowing effect, since the shadowing length is increased as the incoming particles reach the substrate under a flatter angle. Hence, more space is created between the columns so that the inter-columnar distance is enlarged. Moreover, the SEM side-view images show that the thin films consist of tilted columns oriented toward the incoming particle flux. **Table 1** summarizes the obtained columnar tilt angles β depending on the angular positions θ_{OAD} of the sample holder.

Table 1. Tilt angles, inter-columnar distances, and RMS data for varying incidence angles.

θ_{OAD} [°]	74	80	82	86
Tilt angle β [°]	57 ± 1	58 ± 1	59 ± 1	61 ± 1
Intercolumnar distance				
in x-direction [nm]	19 ± 4	21 ± 4	21 ± 6	22 ± 4
in y-direction [nm]	26 ± 6	30 ± 6	29 ± 6	29 ± 7
RMS [nm]	1.441	1.811	1.960	2.327

Two observations can be made. First, all measured tilt angles are smaller than the incidence angles. This observation is well-known and has been confirmed by a large number of experiments, but the detailed dependence of both angles is still in the focus of research.[36–39] Second, the columnar tilt angles are merely enlarged for more oblique deposition geometry from $\beta = 57°$ ($\theta_{OAD} \approx 74°$) to $\beta = 61°$ ($\theta_{OAD} \approx 86°$). This is caused by the oblique deposition geometry, which forces the columns to grow toward the direction of the incoming particle flux. Thus, a more oblique incidence angle leads to an enlarged tilt angle of the columns. However, the large beam divergence and the high working pressures of approximately 10^{-2} Pa influence film growth, because the trajectories of the sputtered particles cannot be considered as parallel. Further, the sputtered particles have, compared to a particle beam created by evaporation, high kinetic energies when arriving at the substrate. This can be sufficient to initiate atomic mobilization processes at the substrates surface, resulting in an information loss concerning the incidence direction of the sputtered particle.[40] However, from the SEM images it can be assumed that the shadowing effect caused by the OAD geometry is still dominating, thereby facilitating the growth of tilted columnar structures on the substrate surface.

From the SEM top views, inter-columnar distances of neighbored columns are measured perpendicular (x-direction) and parallel (y-direction) to the projected tilt direction of the nanostructures (for illustration see Figure 1). The results are summarized in Table 1. The inter-columnar distances tend to increase slightly with more oblique deposition angles for both x- and y-direction. A closer inspection of Table 1 reveals that the inter-columnar distances are larger in y-direction compared to the x-direction. This can be understood by the shadowing effect that appears only in y-direction (along the incoming particle flux). In contrast, shadowing has no impact in x-direction so that the columns grow broadened in that direction, which can result in coalescence. To conclude, the shadowing effect has an

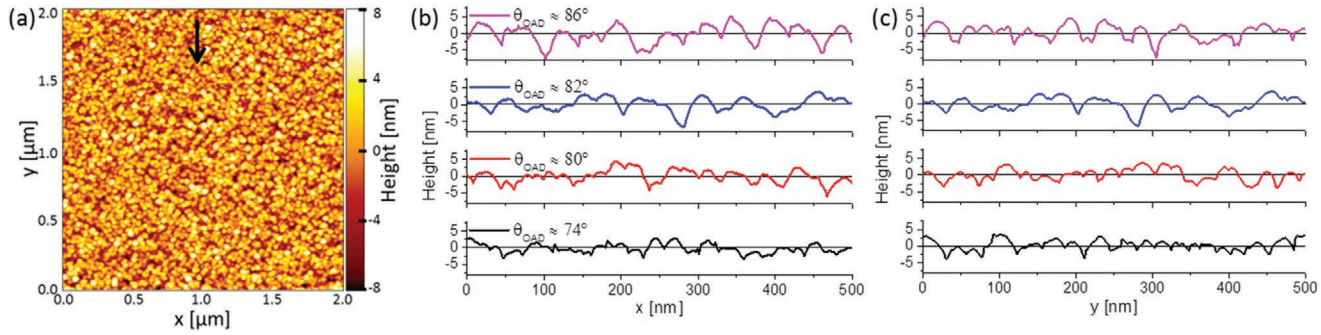

Figure 2. AFM image showing the surface topography for a nanostructured Ti thin film deposited at $\theta_{OAD} \approx 82°$ a). The black arrow indicates the direction of the incoming particle flux. AFM height profiles of nanostructured Ti thin films deposited at $\theta_{OAD} = 86°$, 82°, 80°, and 74°, respectively, measured in b) x- and c) y-direction.

impact on the local topography of the TiO_2 thin film. Additionally, this is also expected to result in an anisotropic rigidity of the substrate, which might have an effect on the cellular migration, as previous studies have already indicated.[16,41–43]

The topography of the nanostructured TiO_2 thin films is further analyzed by AFM measurements. **Figure 2**a depicts the (2D) AFM images exemplarily for a TiO_2 thin film deposited at $\theta_{OAD} \approx 82°$. The image is acquired for a (2×2) µm^2 area. The direction of the incoming particle flux is indicated by the black arrow. Darker regions represent areas with lower height values (with respect to the substrates normal) and indicate shadowed areas. Brighter regions display larger height values. Figure 2b,c depict the AFM height profiles of the TiO_2 thin films deposited at $\theta_{OAD} \approx 86°$, 82°, 80°, and 74°, respectively. Such profiles were measured perpendicular (x-direction) and parallel (y-direction) to the projected tilt direction of the nanostructures (see Figure 2a).

In general, a comparison of the height profiles reveals that for more oblique deposition geometry, the TiO_2 thin films exhibit a roughened surface. This increased surface roughness, also specified in Table 1, is a consequence of the competitive growth process among the developing columns. Caused by the oblique deposition geometry, faster growing nano-sized columns will shadow slower growing columns so that the latter stop developing. In the progress of this evolutionary selection process among the developing columns, only the columns with the fastest vertical growth component (parallel to the substrate normal) will be successful.[44] This process is intensified as the substrate is tilted to more oblique angles, leading to a reduction of the total number of growing columns per unit area, as well as, to an increase of the distance between neighboring columns in y-direction so that the surface roughness is enlarged. In addition, it should be mentioned, that the samples were analyzed by X-ray diffraction (XRD). It was found that all samples show anatase TiO_2.

2.2. Cultivation of C3H-Mice Fibroblasts on the TiO_2 Thin Films

The angle-dependent movements and velocities of L929 fibroblasts are studied in vitro exemplarily on tilted TiO_2 nanostructures with angular positions deposited at $\theta_{OAD} \approx 82°$ and $\theta_{OAD} \approx 74°$ (deposited on fused silica substrates at room temperature) and on smooth TiO_2 substrates. These two angle-dependent samples are chosen because of their surface topography; $\theta_{OAD} \approx 74°$ shows a more even surface (and not that rough) compared to $\theta_{OAD} \approx 82°$. The surface topography of the smooth substrate is more homogeneous and much smoother than the tilted samples. Usage of culture inserts allowed the precise definition of the cell-covered substrate area from the cell-free substrate area (see **Figure 3**). As the inserts are removed, there is a well-defined boundary between cell-covered and cell-free substrate area, thus allowing the observation of cellular activity from a specified starting point after a defined incubation time. As can be observed from Figure 3, movements of single cells as well as collective migration can be observed during the entire observation time up to 28.5 h.

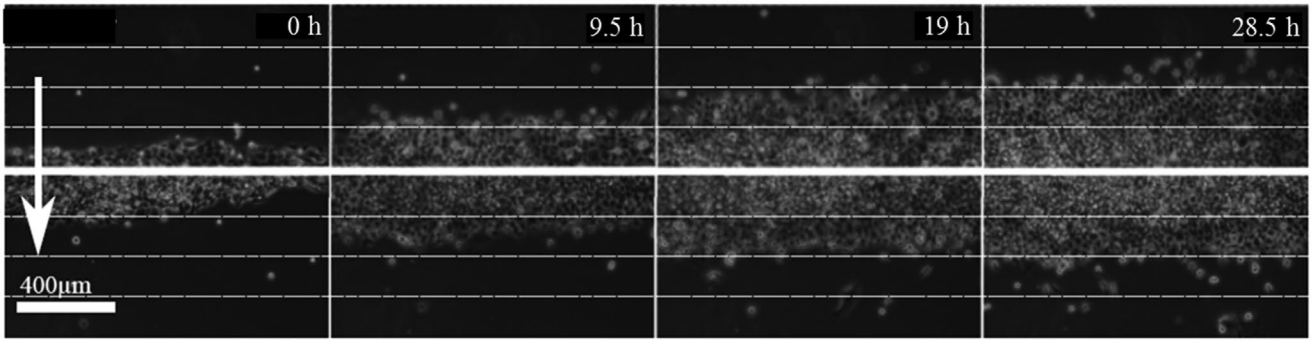

Figure 3. Long-term light microscope observation images of L929 fibroblasts cultured on a nanostructured TiO_2 thin film deposited at $\theta_{OAD} \approx 82°$ shown at distinct observation times. The white arrow indicates the projected tilt direction of the nanostructures.

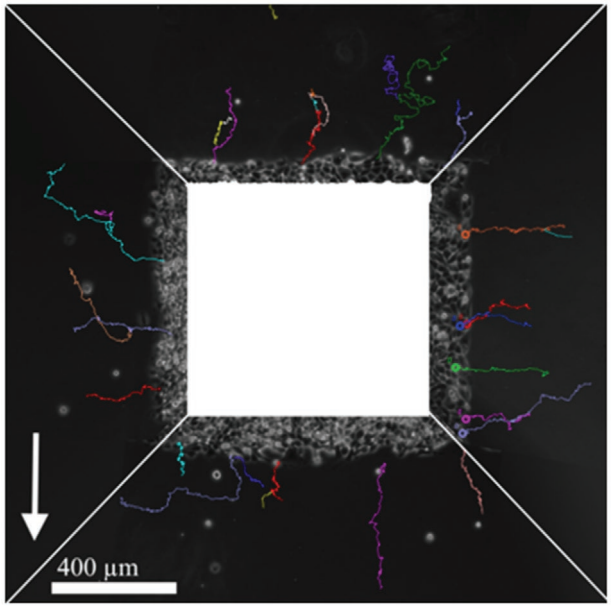

Figure 4. Light microscope image composed of four individual images for tracking the cellular migration paths of L929 fibroblasts in positive and negative x- and y- direction, respectively. The white arrow indicates the projected tilt direction of the nanostructures. Only fibroblasts that were directly located at the boundary between cell-covered and cell-free substrate area have been chosen for this analysis.

Due to cell proliferation, the number of adherent cells significantly increases with incubation time. Even after 40 h after removing the culture insert, smaller and round moving cells, as well as, larger flat cells with filopodia are observable, which allows the assumption of viable and adherent fibroblasts (not shown here). Observing only cells at the boundary, it is possible to identify leader cells that are followed by several cells at the former culture insert boundary and start a collective movement, while other cells move alone. However, analyzing the cell migration depending on the local surface topography requires tracking of individual cell migration paths.

Figure 4 shows a summarized image of individual migration paths of several fibroblasts on a nanostructured sample. The initial cell boundary corresponds in its orientation to the former cell culture insert boundary and was oriented in a way, that a parallel and vertical cell boundary to the tilted TiO_2 columns could be observed. Cells have been tracked along and against the positive and negative x- and y-direction, respectively, and these results are combined for the parallel and vertical cell boundary direction (former insert boundary) to the tilt direction.

From the migration paths of individual cells, we determined the directional distribution, as well as, the velocity distribution in dependence of the directional movement, to characterize cell migration for different directions on the nanostructured TiO_2 thin films in more detail. These results are depicted in **Figure 5**. Here, we clearly see that the cells on top of the deposited at $\theta_{OAD} \approx 82°$ sample strongly prefer to move along the column tilt direction when they started from the vertical boundary (which is equal to top and bottom in Figure 4). Other directions of movement occur but are less present. Cells from the parallel boundary (which corresponds to right and left handside in Figure 4) move equally frequently in x- and y-directions. On the $\theta_{OAD} \approx 74°$ sample this behavior is not pronounced. The cell movement from the parallel boundary is similar to the deposited at $\theta_{OAD} \approx 82°$ sample and complies the isotropic reference sample on a smooth TiO_2 thin film. Cell movement from the vertical boundary is mainly pronounced in three directions, with evenly occurring frequencies. These frequencies are in the same range as for the reference sample without showing significant differences. Direction-dependent cell movement on the smooth TiO_2 sample is evenly distributed. These results indicate that a targeted cell movement can be induced and is dependent of angle of inclination of the TiO_2 columns.

Cell velocities on the smooth sample show no direction-dependence, nor can any dependence be observed on the $\theta_{OAD} \approx 74°$ sample. In contrast, cells on the sample deposited at $\theta_{OAD} \approx 82°$ show a clear velocity loss along the column tilt. This corresponds to a velocity reduction of 40%. The absolute cell velocities are highest on the sample deposited at $\theta_{OAD} \approx 74°$ and lowest on the sample deposited at $\theta_{OAD} \approx 82°$ (see **Table 2**). These results suggest that a targeted cell movement is accompanied by low cell velocities.

A significant difference of the initial parallel to vertical oriented cell boundary within the samples could not be found. Also, the cell boundary velocities hardly differ among each other, as shown in Figure 5.

Cell areas and cell division rates are an indicator for detecting whether cells are vital and are feeling comfortable on the substrate. For this purpose, we determined both parameters for several cells, depicted in **Figure 6**. The mean values are included in Table 2. Cell area of L929 fibroblasts cultured on the sample deposited at $\theta_{OAD} \approx 82°$ is significant smaller than on the sample deposited at $\theta_{OAD} \approx 74°$ and smooth samples. Average cell areas on the $\theta_{OAD} \approx 74°$ sample and smooth samples do not differ from each other. Cells divide fastest on the $\theta_{OAD} \approx 82°$ sample and slowest on the $\theta_{OAD} \approx 74°$ sample. Nevertheless, cell areas and cell division rates are in a normal range for this cell type. It is noticeable that very large cell areas were observed more often on the nanostructured samples with tilted columns. While largest cells on the smooth samples have areas of ≈5 µm^2, cell areas up to 40 µm^2 occurred about three times more often on the tilted column samples.

To conclude, the different inter-columnar distances in x- and y-direction on the nanostructured TiO_2 thin films, as well as, their anisotropic rigidity significantly influence the migration paths of L929-mice fibroblasts. The nanostructures on the $\theta_{OAD} \approx 74°$ sample was not able to influence the cultured fibroblasts, but so does the $\theta_{OAD} \approx 82°$ sample. In contrast to Motemani et al., who cultured human mesenchymal stem cells on TiO_2 nanostructures that have been fabricated by glancing angle sputter deposition, we see that under certain conditions a targeted cell movement is possible.[45] These results are consistent with Jiang et al., who have shown that the migration of mammalian cells can be directed by using asymmetric micropatterned substrates.[19] Also, our experiments are performed with fibroblasts, so this could be a reason for the different cell responses reported by Motemani et al. although

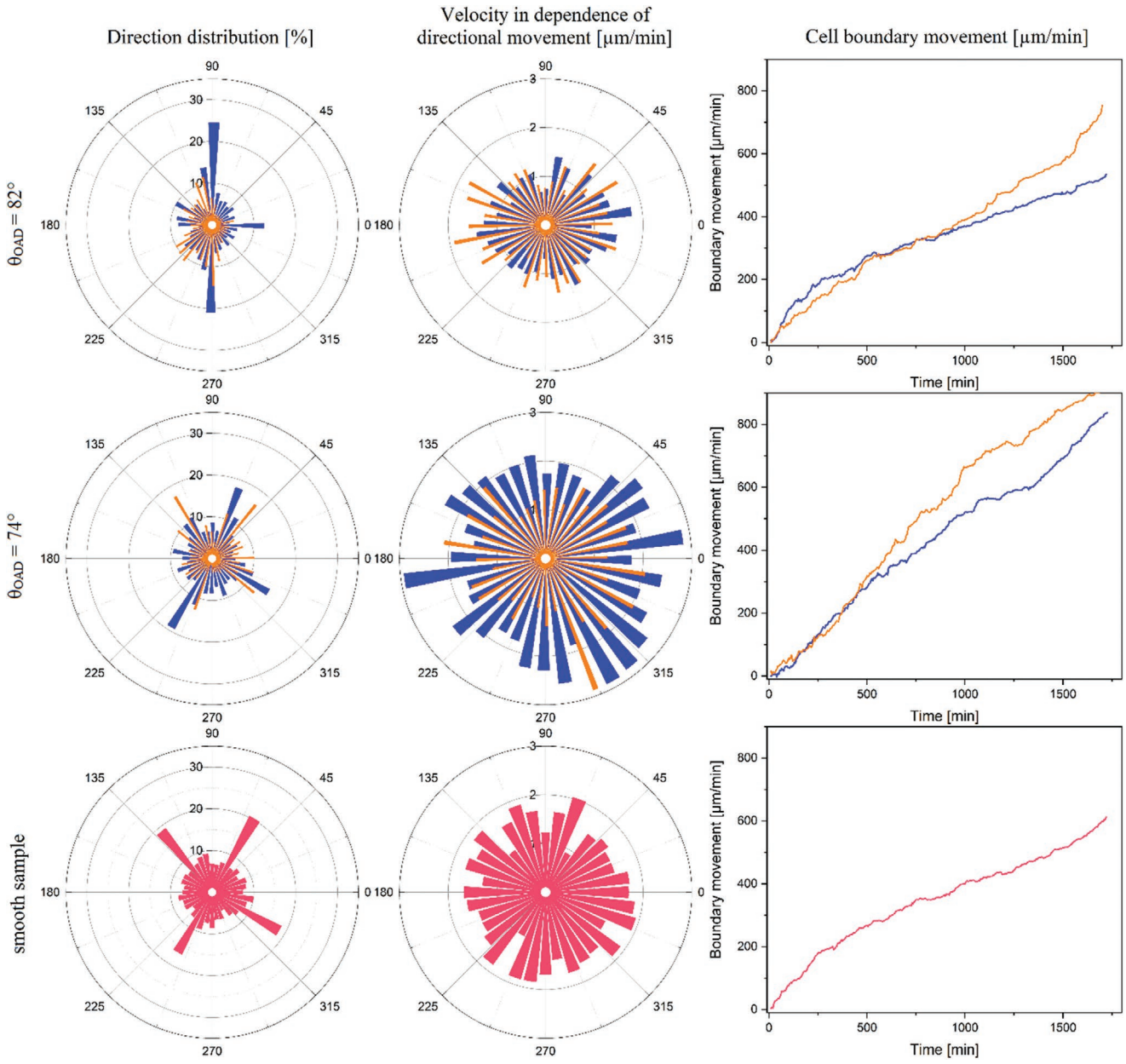

Figure 5. Direction and velocity distributions of single cells, as wells as cell boundary movement on nanostructured TiO_2 thin films deposited at $\theta_{OAD} \approx 82°$, $\theta_{OAD} \approx 74°$ and on smooth TiO_2 over 28.5 h incubation time. Negative and positive x- and y-directions (depending on the cell boundary) are combined so that the cell boundary is parallel in x-direction (orange) and vertical in y-direction (blue) to the column tilt. Cells on the smooth samples have no tilted columns and are shown in pink.

the substrates show amazing similarities. In addition, other nanostructures such as, TiO_2 nanotubes are of particular interest. These surfaces are also biocompatible and by targeted surface modification cell processes can be triggered as shown by Khrunyk et al. They found that cell morphology, adhesion, proliferation, and osteogenic marker expression were affected by their amorphous and anatase nanotube substrates compared to a flat titanium substrate, providing strong evidence that nanostructured substrates are sufficient for inducing osteogenic differentiation.[23]

Table 2. Cell velocities, cell areas, and cell division rates on the distinct nanostructured and smooth TiO_2 thin films.

θ_{OAD} [°]	82	74	Smooth
Velocities [µm min^{-1}]	01.18 ± 0.41	01.81 ± 0.67	01.59 ± 0.43
Cell areas [µm^2]	01.98 ± 0.64	03.07 ± 1.09	02.53 ± 0.68
Cell division rate [h]	16.76 ± 5.67	20.85 ± 7.01	17.21 ± 7.63

In summary, adhesion and proliferation of L929-fibroblasts confirms the biocompatibility of the investigated TiO_2 nanostructured thin films. A directed cell migration behavior

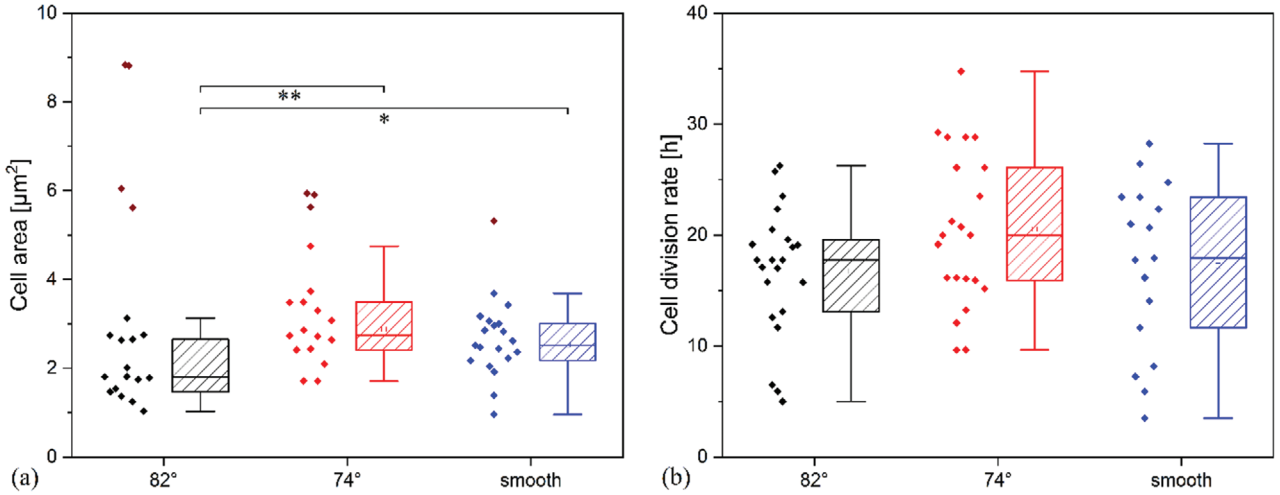

Figure 6. Analyses of a) cell area and b) cell division rate for single cells on distinct TiO_2 samples: TiO_2 columns deposited at $\theta_{OAD} \approx 82°$ and $\theta_{OAD} \approx 74°$ and on smooth TiO_2 thin films. Dark red points in (a) show outliers. Statistical significances are shown (if applicable), where * and ** marked significances at different *p*-values for $p \leq 0.05$ and $p \leq 0.01$, respectively.

could be detected for the $\theta_{OAD} \approx 82°$ sample. Especially, the combination of the biocompatibility and the large surface-area of nanostructured TiO_2 thin films could be of interest for medical applications. For instance, such highly porous surfaces can have an antibacterial effect and might be able to soak fluids such as, antibiotics efficiently to reduce the risk of infections upon implantation in the human body. Furthermore, pseudopodia of fibroblasts might grow in the space between those separated columns, thereby potentially improving the tissue-implant interaction.[45,46]

3. Summary and Conclusion

TiO_2 nanostructured thin films have been fabricated by ion beam sputtering OAD on natively oxidized and fused silica substrates at room temperature and for varying angles of the incoming particle flux. It has been observed that the columnar tilt angles and the roughness of the film are enlarged with more oblique deposition geometry. The inter-columnar distances between neighbored nanostructures tend to increase slightly as the angle of the incoming particle flux is enlarged. Further, the inter-columnar distances are observed to be larger along the projected tilt direction of the nanostructures compared to those located perpendicular to the tilt direction of the nanostructures, which originates from the shadowing effect. Further, it could be demonstrated that fibroblasts adhere and proliferate in vitro on obliquely deposited TiO_2 thin films. We found significant differences in the cellular migration pathways depending on the local surface topography. With higher inter-columnar distances between neighbored columns a directed movement pattern was observed. This directed cell migration is accompanied with a velocity slowdown. Cell areas and cell division rates indicate biocompatibility of the deposited nanostructured TiO_2 thin films. Hence, such films might be promising candidates for medical applications such as, Ti-based implants by modifying and improving their production parameters. For future research, the ability to produce nanostructured thin films with predictable surface properties bears the potential to open a new pathway for understanding biological interactions between implant surfaces and tissue.

4. Experimental Section

Fabrication and Characterization of Nanostructured TiO_2 Thin Films: The TiO_2 nanostructured thin films were grown by reactive ion-beam sputtering using a metallic Ti target (purity 99.99%), a constant Ar flux (6.5 sccm) sustaining the plasma in the ion beam source and a constant O_2 flux (3 sccm) as process gas. The base pressure in the deposition chamber was 10^{-4} Pa, while the working pressure was constant at 2.5×10^{-2} Pa. The deposition rate varied between 0.3 and 0.8 nm min^{-1} depending on the position of the sample holder with respect to the incoming particle flux. The film thickness (measured parallel to the substrate normal) was controlled by the deposition time. Natively oxidized, p-doped Si(100) pieces and fused silica pieces were used as substrates. The substrate area was roughly (1×1) cm^2. The distance between sample holder and Ti target was ≈15 cm. The Ti target was 15 cm in diameter and the beam size on the target was 10 cm. Consequently, the Ti atoms are emitted in an angular distribution typical for the sputtering process. Thus, the incoming particle flux on the substrate (or growing film) is characterized by this angular distribution. Cross-sectional images of the samples were obtained by cleaving the samples before investigation with SEM at 10 kV acceleration voltage. Here, secondary electrons were used. The tilt angles of the grown nanostructures (obtained from the cross-sectional SEM images) as well as, the distance between neighboring nanostructures (obtained from the top-view SEM images) were measured manually.

To study the roughness of the tilted titanium dioxide columns, an Icon AFM (Bruker) was used. Silicon OTESPA R.3 tips with a tip radius of 7 nm were used in tapping mode. In the tapping mode, the distance of the tip to the surface changes and thus the applied force does. Measurements were performed at constant amplitude and a resonance frequency of 300 kHz. An area of 2 µm x 2 µm was scanned in each case.

Cell Cultivation and Data Analysis of Cellular Velocities and Morphology on Nanostructured TiO_2 Thin Films: L929 cells (derivative of Strain L) were purchased from ATCC. L929 cells were incubated in usual cell culture flasks and in complete cell culture medium (90% Roswell

Park Memorial Institute RPMI and 10% fetal calve serum) at 5% CO_2 atmosphere and 37 °C. Cells were passaged when they reached a confluency of 80%. Fibroblasts were counted with a hemocytometer and seeded with a concentration of 4.6×10^4 cells mL^{-1} per well of a culture insert (2 Well in µ-Dish, growth area of 0.22 cm^2, Ibidi), which was placed onto smooth (reference sample) and nanostructured TiO_2-samples. Thereby, the culture inserts were oriented perpendicular to the projected tilt direction of the nanostructures. Total cell culture volume within one well was 50 µL. Prepared samples were cultured under the same culture conditions as single cells in normal culture flasks as described above. For long-term investigations, 5% antibiotic Gentamicin was added to the cell medium. Phase contrast images were recorded every 5 min for up to 40 h after seeding using a Leica DM IRB phase contrast microscope in a thermo box case and a 10 x-objective. During the observation time, the temperature was kept constant at 37 °C and CO_2 was inserted continuously to ensure a 5% CO_2 atmosphere. In principle, longer observation was possible, but not recommended, because most of the cells moved out of focus. Therefore, results were only shown until 28.5 h after removing the cell culture insert. The traveled distance of the cells after removing the inserts was measured with video analysis and the modeling tool software Tracker.[47] Exemplary, 5 to 10 cells were tracked on each cell boundary and their ways were followed by marking their positions in the individual phase contrast images over time. Simultaneously, the movement of the cell boundary was analyzed. From these data, cell and boundary velocities were determined. In order to obtain direction and velocity distributions, the positive and negative x- and y-directions were combined into parallel and vertical directions along the column tilts. Each migration path of a single cell was color encoded. If a cell had undergone cell division during migration, the migration path of one of the new cells had been encoded in another color. These time stamps were used to determine the cell division rate. Cell areas were evaluated using Fiji. Here, the perimeter of the single cells was manually determined, the enclosed number of pixels was subsequently counted, and the cell area was calculated using the conversion factor from microscope and objective.

Acknowledgements

U.K. and S.F. contributed equally to this work. The authors acknowledge Prof. Josef Käs, Division of Soft Matter Physics, University of Leipzig for sharing the long-term cell investigation setup and Dr. Philipp Schumacher, IOM, for conducting the AFM measurements. Funding by the Deutsche Forschungsgemeinschaft (DFG) Astrid Kupferer acknowledges funding for a scholarship of the Heinrich Böll foundation as well as, the BMBF-Project EYECULTURE (FKZ 161A574C/031A574C) is gratefully acknowledged.

Open access funding enabled and organized by Projekt DEAL.

Conflict of Interest

The authors declare no conflict of interest.

Data Availability Statement

The data that support the findings of this study are available from the authors upon reasonable request.

Keywords

directed cell migration, oblique angle sputtering deposition, proliferation, tilted columns, TiO_2 nanostructures

Received: April 19, 2021
Revised: June 18, 2021
Published online: August 7, 2021

[1] M.-P. Alvarez, I.-B. González, R. Fernández-Martínez, G.-V. Arcos, V.-R. Palmero, G.-M. González-Elipe, *Nanomaterials* **2019**, *9*, 1217.
[2] A. Barranco, A. Borras, A. R. Gonzalez-Elipe, A. Palmero, *Prog. Mater. Sci.* **2016**, *76*, 59.
[3] M. M. Hawkeye, M. T. Taschuk, M. J. Brett, *John Wiley & Son* **2014**, 173.
[4] D. Rafieian, W. Ogieglo, T. Savenije, R. G. H. Lammertink, *AIP Adv.* **2015**, *5*, 097168.
[5] R. C. Jayasinghe, A. G. U. Perera, H. Zhu, Y. Zhao, *Opt. Lett.* **2012**, *37*, 4302.
[6] E. Manea, C. C. Parvulescu, M. Purica, E. Budianu, F. Comanescu, *J. Nano Res.* **2012**, *21*, 89.
[7] W. Maziarz, A. Kusior, A. Trenczek-Zajac, *Beilstein J. Nanotechnol.* **2016**, *7*, 1718.
[8] Y. Pihosh, I. Turkevych, J. Ye, M. Goto, A. Kasahara, M. Kondo, M. Tosa, *J. Electrochem. Soc.* **2009**, *156*, K160.
[9] M. Suzuki, T. Ito, Y. Taga, *Appl. Phys. Lett.* **2001**, *78*, 3968.
[10] C. Dumitriu, M. Popescu, C. Ungureanu, C. Pirvu, *Appl. Surf. Sci.* **2015**, *341*, 157.
[11] J. Rosenbaum, D. L. Versace, S. Abbad-Andallousi, R. Pires, C. Azevedo, P. Cénédese, P. Dubot, *Biomater. Sci.* **2017**, *5*, 455.
[12] S. Brown, J. Lemons, *Medical Application of Titanium and its Alloys: The Material and Biological Issues* (Eds: S. Brown, J. Lemons), ASTM International, West Conshohocken **1996**.
[13] D. M. Brunette, *Titanium in Medicine Material Science, Surface Science, Engineering, Biological Responses and Medical Applications* (Eds: D. M. Brunette, P. Tengvall, M. Textor, P. Thomsen), Springer, Berlin **2001**, pp. 485–512.
[14] X. Liu, P. Chu, C. Ding, *Mater. Sci. Eng., R* **2004**, *47*, 49.
[15] R. L. d. Miranda, C. Zamponi, E. Quandt, *Smart Mater. Struct.* **2009**, *18*, 104010.
[16] M. Lampin, N. Warocquier-Clérout, C. Legris, M. Degrange, M. F. Sigot-Luizard, *J. Biomed. Mater. Res.* **1997**, *36*, 99.
[17] W. Zhou, X. Zhong, X. Wu, L. Yuan, Z. Zhao, H. Wang, Y. Xia, Y. Feng, J. He, W. Chen, *Surf. Coat. Technol.* **2006**, *200*, 6155.
[18] S. Lavenus, J.-C. Ricquier, G. Louarn, P. Layrolle, *Nanomedicine* **2010**, *5*, 937.
[19] X. Jiang, D. A. Bruzewicz, A. P. Wong, M. Piel, G. M. Whitesides, *Proc. Natl. Acad. Sci. U. S. A.* **2005**, *102*, 975.
[20] A. W. Tan, B. Pingguan-Murphy, R. Ahmad, S. A. Akbar, *Ceram. Int.* **2012**, *38*, 4421.
[21] F. Vetrone, F. Variola, P. T. d. Oliveira, S. F. Zalzal, J.-H. Yi, J. Sam, K. F. Bombonato-Prado, A. Sarkissian, D. F. Perepichka, J. D. Wuest, F. Rosei, A. Nanci, *Nano Lett.* **2009**, *9*, 659.
[22] J. Park, S. Bauer, K. von der Mark, P. Schmuki, *Nano Lett.* **2007**, *7*, 1686.
[23] Y. Y. Khrunyk, S. V. Belikov, M. V. Tsurkan, I. V. Vyalykh, A. Y. Markaryan, M. S. Karabanalov, A. A. Popov, M. Wysokowski, *Nanomaterials* **2020**, *10*, 320.
[24] N. G. Durmus, T. J. Webster, *Nanomedicine* **2012**, *7*, 791.
[25] F. Variola, J. B. Brunski, G. Orsini, P. T. d. Oliveira, R. Wazen, A. Nanci, *Nanoscale* **2011**, *3*, 335.
[26] L. S. Nair, C. T. Laurencin, *J. Bone Jt. Surg., Am. Vol.* **2008**, *90*, 128.
[27] R. Langer, D. A. Tirrell, *Nature* **2004**, *428*, 487.
[28] J. M. Holzwarth, P. X. Ma, *J. Mater. Chem.* **2011**, *21*, 10243.
[29] V. Beachley, X. Wen, *Prog. Polym. Sci.* **2010**, *35*, 868.
[30] M. M. Hawkeye, M. T. Taschuk, M. J. Brett, *John Wiley & Son* **2014**, 31.
[31] V. Torrisi, F. Ruffino, *Surf. Coat. Technol.* **2017**, *315*, 123.
[32] H. Vankranenburg, C. Lodder, *Mater. Sci. Eng., R* **1994**, *11*, 295.
[33] L. Abelmann, C. Lodder, *Thin Solid Films* **1997**, *305*, 1.
[34] A. Dolatshahi-Pirouz, C. P. Pennisi, S. Skeldal, M. Foss, J. Chevallier, V. Zachar, P. Andreasen, K. Yoshida, F. Besenbacher, *Nanotechnology* **2009**, *20*, 095101.
[35] C. P. Pennisi, A. Dolatshahi-Pirouz, M. Foss, J. Chevallier, T. Fink, V. Zachar, F. Besenbacher, K. Yoshida, *Colloids Surf., B* **2011**, *85*, 189.

[36] B. Tanto, G. T. Eyck, T.-M. Lu, *J. Appl. Phys.* **2010**, *108*, 026107.
[37] R. N. Tait, T. Smy, M. J. Brett, *Thin Solid Films* **1993**, *226*, 196.
[38] J. Nieuwenhuizen, H. Haanstra, *Philips Tech. Rev.* **1966**, *27*, 87.
[39] C. Grüner, S. Liedtke, J. Bauer, S. G. Mayr, B. Rauschenbach, *ACS Appl. Nano Mater.* **2018**, *1*, 1370.
[40] T. Smy, M. Salahuddin, S. K. Dew, M. J. Brett, *J. Appl. Phys.* **1995**, *78*, 4157.
[41] A. Majeed, J. He, L. Jiao, X. Zhong, Z. Sheng, *Nanoscale Res. Lett.* **2015**, *10*, 56.
[42] J. Lincks, *Biomaterials* **1998**, *19*, 2219.
[43] A. Saez, M. Ghibaudo, A. Buguin, P. Silberzan, B. Ladoux, *Proc. Natl. Acad. Sci. U. S. A.* **2007**, *104*, 8281.
[44] A. V. D. Drift, *Philips Res. Rep.* **1967**, *22*, 267.
[45] Y. Motemani, C. Greulich, C. Khare, M. Lopian, P. J. S. Buenconsejo, T. A. Schildhauer, A. Ludwig, M. Köller, *Appl. Surf. Sci.* **2014**, *292*, 626.
[46] J. Hasan, R. J. Crawford, E. P. Ivanova, *Trends Biotechnol.* **2013**, *31*, 295.
[47] D. Brown, R. Hanson, W. Christian, Tracker Video Analysis and Modeling Tool, Version 5.1.5, https://physlets.org/tracker/ (accessed: November 2020).